

Visual Summary of Value-level Feature Attribution in Prediction Classes with Recurrent Neural Networks

Chuan Wang*
University of California, Davis

Xumeng Wang†
Zhejiang University

Kwan-Liu Ma‡
University of California, Davis

ABSTRACT

Deep Recurrent Neural Networks (RNN) is increasingly used in decision-making with temporal sequences. However, understanding how RNN models produce final predictions remains a major challenge. Existing work on interpreting RNN models for sequence predictions often focuses on explaining predictions for individual data instances (e.g., patients or students). Because state-of-the-art predictive models are formed with millions of parameters optimized over millions of instances, explaining predictions for single data instances can easily miss a bigger picture. Besides, many outperforming RNN models use multi-hot encoding to represent the presence/absence of features, where the interpretability of feature value attribution is missing. We present ViSFA, an interactive system that visually summarizes feature attribution over time for different feature values. ViSFA scales to large data such as the MIMIC dataset containing the electronic health records of 1.2 million high-dimensional temporal events. We demonstrate that ViSFA can help us reason RNN prediction and uncover insights from data by distilling complex attribution into compact and easy-to-interpret visualizations.

1 INTRODUCTION

Deep Recurrent Neural Networks (RNN) is pervasively used in reasoning and decision-making tasks in sequential data analysis. Due to its remarkable performance and broadly applicable feature, RNNs have helped to solve problems in domains from fundamental research such as natural language processing (NLP) [45] and video analysis to domain research such as electronic health records (EHR) analysis [5], customer behavior analysis [43], and stock prediction [2].

Despite RNNs' popularity and remarkable performance, end-users demanding on model *trust*, *fairness* and *reliability* become a limitation in many critical real-world decision-making schemes. One would be critical of a reliability-oriented paper that only cites accuracy statistics [9]. Consciously collected data can be easily biased, and models built with such data can be unreliable. For example, Ribeiro et al. [33] show a case where the snow backgrounds in the training images, instead of real morphological features, distinguishes "huskies" from "wolves". Such problem happen to sequential data analysis too. It will be critical and causing fatal issues if similar problems happened to applications such as health care, autonomous vehicles, or legal matters. How to make sure a model's decision is not based on biased facts? How do we provide trusted prediction systems that humans are confident to use? How do we guarantee the decisions are not discriminated against by a special group? It's urgently demanded to solve these problems and use machine learning models transparently and safely.

To address this subject, existing work has focused on visualizing RNN predictions for domain-specific tasks such as NLP [25, 40] by revealing RNNs' inner mechanisms. However, RNN models

have a broader usage in various scientific research fields such as DNA sequence analysis [30], electronic health records (EHR) analysis [5], customer purchase intent analysis [36], stock prediction [2]. Explanations in domain-specific manners can not fulfill the requirements in diverse scenarios. For example, word-to-vector embeddings in the NLP domain are fundamentally different from one-hot or multi-hot embeddings in most applications where each embedding vector dimension has physical meaning. Owing to this difference, the visual analysis for the NLP domain can be distinctive among general visual analysis with RNN predictions. Besides, interpreting inner-model behavior can be fragmentary in real practice and can potentially cause catastrophic harm to society [35]. Furthermore, it's important for humans to understand and trust a model's predictions by knowing how multi-dimensional features and their temporal changes in entire prediction classes contribute to prediction. Current visual interpretations often focus on explaining predictions for individual instances [19, 27]. Because deep learning models are computed based on a populous distribution of instances, explanations for individual instance prediction can easily miss a bigger picture of important insights learned by a model. Last, **value-level feature attribution** is not previously addressed for model interpretation, yet explaining what values in a feature contribute to a particular class would be more meaningful than simply illustrating whether a feature has a high contribution. For example, knowing the importance of feature "customer visits" would provide less guidance than telling how many visits would be effective in preserving customers. Therefore, it's often desirable to explain models by visualizing **temporal feature value attribution for the entire prediction classes in a domain-independent manner**.

Our work is inspired by these unfulfilled requirements and attempts to resolve the following challenges. *Data complexity*: datasets for RNN modeling can be seen as tensors that composed of time, multi-dimensional feature, and instance. In the settings of RNN modeling, each instance is a sequence, and is labeled with a class. For example, in the patient mortality analysis, a patient's medical temporal history is associated with a mortality label dead/alive. At each time-step, a temporal event is composed of multi-dimensional features representing values from medications, lab test results, etc. Despite the complexity in data rank and dimension, analysing such practical data often desires handling of specialties such as sparsity and noisiness. *The dilemma – generality or visual complexity*: Complex visualizations systems are often tailor-made for specific data characteristics or analytic tasks, and high generality requirements often limit possible visualization designs. We aim to handle compound computation at the backend in exchange of an easy-to-comprehend visualization designs for a RNN-model-agnostic straightforward interpretations of data insights. We introduce ViSFA which visually summarizes feature attribution with RNNs and provides:

- A scalable and domain-independent visual analytics approach that summarizes feature attribution in entire prediction classes. We designed a series of modular algorithms based on stratified sampling and gap statistic clustering, which facilitate a fair comparison of contributing patterns in temporal value change between classes.
- An **interactive** visualization system for users to remove irrelevant noises and discover major contributing sequential patterns.

*e-mail: nauhcy@gmail.com

†e-mail: wangxumeng@zju.edu.cn

‡e-mail: ma@cs.ucdavis.edu

2 RELATED WORK

A deep neural network is typically trained with a large number of instances that each is annotated with a class label. A well-trained deep learning model can learn useful knowledge from the instances and form a complex network of neurons that transform the instances to a probability for class prediction. However, how deep neural networks learn knowledge and achieve outperform predictions are remained unclear. Researchers from both the Machine Learning and Data Visualization field have investigated the interpretability of deep learning models. However, there is not a single interpretation method that can be applied to any deep learning models [9].

2.1 RNN Model interpretation

Currently, there are two major approaches in terms of whether RNN models are extended for interpreting deep learning models.

To interpret the dynamics of deep neural networks, a few studies apply visual approach to explain convolutional neural networks [3,10,14,32,39]. For understanding RNNs, model-generating factors, like hidden states, need to be explored. LSTMVis [40] visualizes the hidden state dynamics of RNNs by a parallel coordinates plot. To match similar top patterns, LSTMVis allows users to filter the input range and check hidden state vectors from heatmap matrices. For natural language processing tasks, Ming et al. [25] also employ a matrix design. Combining hidden state clusters and word clusters, Ming et al. [25] design a co-clustering layout, which links cluster matrices and word clouds.

In addition, extending RNNs by extra structures, like neural attention mechanisms, contributes to easier interpretation. The attention mechanism has become popular recently because the added attention layers allow the interpretation of a particular aspect of the input [1, 12, 44]. Besides, the attention mechanism is proved to be able to improve the performance of deep learning models. Hermann et al. [12] develop an attention-based method for deep neural nets for comprehending documents. Due to easier interpretation for end-users, this group of research is often applied to real-world analysis in a variety of domains. However, only a few works focus on the visual interpretation of deep learning with an attention mechanism. RetainVis [19] is a rare example that is an interpretable and interactive visual analytics tool for EHR data.

2.2 Additive Feature Attribution Methods

The highest accuracy for large modern datasets is often achieved by complex models that even experts struggle to interpret. To simplify model understanding, a branch of research uses additive feature attribution methods that consider deep learning models as black boxes and explain simpler explanation models as approximations of the original model. Model-specific approximation such as DeepLIFT [37, 38] compares the activation of each neuron to its “reference activation” and assigns contribution scores according to the difference. There are also model-agnostic methods such as LIME [33] and SHAP [21]. LIME interprets individual model predictions based on locally approximating the model around a given prediction. SHAP use Shapley values as a measure of feature variable contribution towards the prediction of the output of the model. Simpler explanations improves computational performance for interpretation. Similar in spirit, Manifold [46] provides a visual analysis framework to support interpretation, debugging, and comparison of machine learning models. These approaches differ from our work in that they approximate RNN models with simpler explanation models, whereas we attempt to interpret the behavior of original models.

2.3 RNN Application fields

RNN becomes popular for its high performance in the linguistic domain. Most well-known works are from the NLP field, such as machine translation and sentiment analysis [15]. Due to the popularity of NLP tasks, the majority of RNN interpretation work has made

efforts to explain RNN models under the NLP background, such as [8, 20, 25, 40]. However, the visual analysis of NLP often requires special visualization techniques because language composed by individual words is a unique type of data. The architecture of RNN is distinctive because connections between nodes form a directed graph along a temporal sequence. Therefore, RNN can be used to a broad range of sequence analysis applications, such as DNA sequence analysis [30], Electronic Health Records (EHR) analysis [5], customer purchase intent analysis [36], stock predictions [2], and so on. As discussed in the introduction, the interpretability is critical to these application domains regarding model fairness, reliability, and trust. However, not much attention has addressed to the visual interpretation of RNN from a more generic perspective except for ProSeNet [26], which proposes an interpretable and steerable deep sequence model.

This paper attempts to bridge this gap and propose a visual analysis method that can be applied to broader scenarios of analyses for summarizing contributing sequence patterns in predictions. Because end-users’ understanding is an urgent desideratum, this work focuses on visualizing distilled patterns that directly map to the original data, based on attention mechanism enhanced RNN model for its easy-to-perceptible superiority. Besides, to our best knowledge, there is no work explaining how RNN models correlate contributing numeric/categorical values with the prediction except Attention-Heatmap [43]. This work extends AttentionHeatmap in the analysis flow and visualization designs.

3 DESIGN CONSIDERATIONS

There are a few observations of RNN models before visualizing feature attribution with them [25, 40, 43]. First, if an RNN model is successfully trained, the instances within a prediction class in the dataset are expected to share some common characteristics which can be captured by the RNN model. In other words, if the instances does not share any common pattern within any prediction class, it’s impractical to learn a convergent or high-performance RNN model. Second, characteristics from different prediction classes are different. If the commonalities from one class can not distinguish itself from another, the model training can not succeed. Third, the attention weight of an event reflect the importance of the event in making such distinction. However, because state-of-the-art RNN models trained with real-world datasets can hardly achieve 100% accuracy, the learned attention weights are often not completely accurate. For example, LSTMVis [40] notices interpretable patterns but also significant noise when studying RNN models. Likewise, AttentionHeatmap [43] reveals that the filtered events contain noise that does not follow the major pattern no matter what attention range is selected by the user.

Based on the above observations, we derive the following design goals (DGs):

DG1: Facilitate the attribution analysis for tensors that are composed of dimensions including time, instance, feature, and feature value. Given multi-dimensional tensors, how do we synthesize meaningful visualizations for interpreting a model’s prediction? Knowing how entire classes share common patterns are not enough because these patterns not necessarily contribute to the model formation, a.k.a, distinguishing different classes. Therefore, the system should help to distill complex data to find the contributing subset and visualize the patterns in the subset.

DG2: Highlight major patterns across the instances within each prediction class. As mentioned earlier, we notices significant noise when studying deep learning models. The learned attention weights are noisy too. The visualization should remove or minimize the influence of noises and highlight major patterns in data. Besides, the visualization should highlight common patterns shared among the instances in a prediction class. Those common patterns are the keys for users to find insights from each class.

DG3: Contrast differences between prediction classes. The visualization design should facilitate easy and fair comparison between different classes. For example, visual comparison based on imbalanced class sizes can suffer from inequity if the visualization results are affected by class sizes. The visualization design should guarantee the visualized pattern is a true reflection of its belonging class instead of the influence of class size.

DG4: Be able to scale for large datasets. Because predictions based on state-of-the-art models are formed with millions of weights optimized over millions of data instances, explaining predictions for single data instances can miss a bigger picture oftentimes. Understanding how entire classes contribute to a model is important for trusting a model’s prediction and deciphering what a model has learned. Therefore, the design should build entire class representations regardless of class size.

DG5: Be generic for different applications. RNN becomes widely used across different domains because of its generality. Even the vanilla RNN models can be adaptive for multiple disciplines such as finance stock price forecasting [2], customer analysis predicting purchasing intent [36]. It’s challenging but meaningful to build a domain-independent visualization system. For users from different domains, we should provide easy-to-interpret interaction and visualization designs.

4 RNN MODEL

This approach leverages LSTM networks with a single-layer attention network. The attention model computes a value that represents the importance of a particular temporal event for every time-step of all instances. Many approaches build end-to-end models for RNN interpretation such as [5, 15]. These methods are not sufficiently developed for the applications that require advanced discussions. Such models often use multi-hot vector feature encoding where 0/1 are used to represent the appear/absence of a feature but without detailed information. For example, in the EHR data analysis, each temporal event is a patient visit. During a patient visit, whether a treatment is performed or a type of medicine is applied is more fundamental. Either use a treatment/medicine or not is more of a standard process, but it’s more meaningful to study how much treatment or the dose of medication can be more effective to a patient group.

This work extends the analysis with these models by using numeric feature encoding so that the analysis result can help to understand the importance of features at different value levels. Instead of multi-hot vector encoding, we train the RNN model with the data encoded with the actual values for the features that are numerical. Because higher granularity of information is used, harder the model can find patterns from the dataset and the model can converge. Therefore, it is more difficult to tune a model with such data encoding. However, by including actual values in the learning process, the analysis can be more practical for studies. In the above example of EHR data analysis, our approach keeps track of the contribution of each feature value. The contribution analysis based on this approach derives insights that can help doctors make future decisions such as what treatment to apply to patients.

5 ViSFA

AttentionHeatmap [43] presents a visual analytics interface for RNN feature attribution analysis, which is composed of the matrix grid view for visualizing time-folded feature attribution, and the k-partite graph view for displaying attribution change over time. The interface of AttentionHeatmap is designed for user groups such as RNN model trainers and data scientists. For ultimate end-users like domain analysts who have no machine learning knowledge, we create ViSFA to help them focus on major patterns distilled from data. For time-folded feature attribution analysis, ViSFA improves AttentionHeatmap by integrating a ranking algorithm that sort features in contribution descending order. ViSFA improves the visual analytics

procedures by providing comparable visual summaries of temporal feature attribution and lets end-users interactively removing noise (DG1). We introduce more details in the following sections.

5.1 Data & Control Flow

We pre-process data so that the time-steps for each instance are aligned reasonably. Each instance x_i in the tensor space $\mathbb{R}_I^{T \times F}$ is a temporal sequence $\{x_i^1, \dots, x_i^{t-1}, x_i^t, x_i^{t+1}, \dots, x_i^T\}$ that is of length T and labeled with a class y_i in the training dataset $D = \{x_i, y_i\}$, where $t \in \{1, T\}$ and $y \in \{1, L\}$ is one of L categorical labels. $f \in \{1, F\}$ is one of F -dimensional features whose value range is $[v_{f_{min}}, v_{f_{max}}]$, and each event x_i^t can be further expanded to a multidimensional expression $\{x_i^{t,1}, \dots, x_i^{t,f-1}, x_i^{t,f}, x_i^{t,f+1}, \dots, x_i^{t,F}\}$ where $x_i^{t,f} \in [v_{f_{min}}, v_{f_{max}}]$. Therefore, the research problem becomes calculating contribution scores s_f for each feature, and visualizing the temporal change in the values of highly contributing features. But how to calculate the contribution of each feature?

Fortunately, the attention mechanism for RNN models is designed to solve the problem. The RNN model training process is using the dataset D to form a complex model $\hat{y}_i = g(x_i)$ where g transforms input data \mathbf{x} to \mathbf{y} using millions of parameters. During the training process, parameters were decided by minimizing a chosen loss function $\sum_{t=1}^T \mathbb{L}_t(y_i^t, \hat{y}_i^t)$. The attention mechanism plugs an attention network to original RNN model and learns a set of parameters $\{a_i^1, \dots, a_i^{t-1}, a_i^t, a_i^{t+1}, \dots, a_i^T\}$ where $a_i^t \in [0, 1]$ represents the importance of each event in the corresponding instance’s temporal sequence. The two-level attention model further computes a set of parameter $\{a_i^{t,1}, \dots, a_i^{t,f-1}, a_i^{t,f}, a_i^{t,f+1}, \dots, a_i^{t,F}\}$ at each temporal event a_i^t for each corresponding feature.

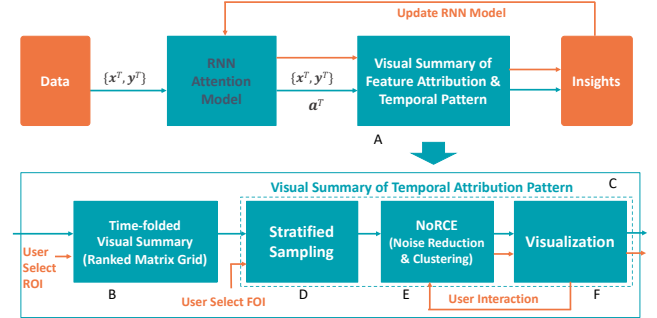


Figure 1: The data flow (green arrows) and the user control flow (orange arrows) passing through a sequence of modules in ViSFA.

As shown in Figure 1, the top row illustrates the high-level flow, where the approach has two components. First, data are feed into the RNN model to train a classifier that can predict the class of a sequence above a user-defined accuracy. The attention mechanism then outputs the attention sequence \mathbf{a}^T . Thereafter, two sets of data from the input of the visualization module: the original data containing instances and their labels $D = \{x_i, y_i\}$ and the attention sequences \mathbf{a}^T that are associated with each temporal sequence and reflects the importance of each temporal event in the sequences.

The visual summary module A is composed of the time-folded summary module (B) and the module for visually summarizing temporal attribution patterns (C). We applied the matrix grid view in AttentionHeatmap [43] as the time-folded summary module. Our work enhances the matrix-grid view with a ranking algorithm that comprehensively computes the contribution of each feature. Then a user would slice the data by distilling temporal events with an attention range of interest (AOI). Specifically, after user selecting AOI, the feature values whose corresponding attention values are outside the AOI becomes “NULL” in the vector representation. In deep learning, empty events are usually padded with zeros for easy

matrix computation. However, in the visual analysis step, padding zeros can be ambiguous because zero values can both represent uninterested events and contributing values. Therefore, the feature f 's value range becomes $\{\emptyset \cup [v_{fmin}, v_{fmax}]\}$. Module C then transforms the filtered data with a sequence of operations D, E, and F, as shown in Figure 1. To fulfill the design goals, we tested several operational and visualization design alternatives and resolved with a series of algorithms that keep users in the loop. We explain the details in the following sections.

5.2 Ranking Feature Contribution

Two factors are taken into consideration when determining the overall contribution score s_f for feature f : the average frequency of all feature values C and the variance V . If the values of f are divided into M bins b_m^f ($m = [1, M]$), the definition of s_f is

$$s_f = C(x^f) * V(x^f) \quad (1)$$

where

$$C(x^f) = \frac{\sum_{m=1}^M |b_m^f|_c}{M} \quad (2)$$

and $V(x^f)$ represents the variance of array x^f . $|x|_c$ represents the cardinality of x . Term C determines whether contributing feature values between classes are profoundly different on average. Term V measures how different the bin values contribute to classification. Therefore the score s_f combines the contribution of feature values and their variations. Because $C > 0$ and $V > 0$, we have $s_f > 0$.

AttributionHeatmap summarize time-folded feature attributions with matrix grids [43]. We extend the matrix grid visualization with a ranking algorithm so that the feature of the highest score is on the top/left and the lowest score on the bottom/right. With the ranking function, users can instantly locate features of interest (FOIs) instead of searching for FOIs by visually comparing matrices in the matrix grid. Users can also interactively select the number of features to remove the features of low contributions.

After users located FOIs, a primary contribution of ViSFA is helping users to compare the contributing sequential patterns between different classes. There are challenges in such visual comparisons, such as different instance sizes in two classes and significant noises in computed feature attribution. We design a series of procedures to solve these problems. As shown in Figure 1, we present these procedures D, E and F in the following sections. We provide a summary of these procedures in Algorithm 1.

5.3 Between-class Comparison – Stratified Sampling

Fair comparisons are prerequisites (**DG3**) when comparing the contributing sequences between entire prediction classes. However, sequences from two prediction classes can be fundamentally different in size, distribution, and contributing values. Visually comparing them by simply aggregating the sequences within each class can be misleading. For instance, a between-class comparison showing the aggregated values for two imbalanced instance sizes can lead to ambiguous because it can be either the values or the instance sizes that causing an overall difference. Besides, the analysis should be scale to summarize temporal patterns from large datasets (**DG4**). Even if the scale of a training dataset reaches or larger than millions, the analysis should still be able to visualize patterns for different classes in the dataset. For a large dataset, a particular scale of aggregation or summarization is essential. Otherwise, the visualization can suffer from a limited canvas size if using a juxtaposed design or a visual blocking if adopting an overlapped design. Additionally, the summary of contributing sequences should be a true reflection of its belonging class.

To meet these requirements, we propose to use a method using stratified sampling after testing a few alternatives, such as random sampling. Stratified sampling is one of the probability sampling

methods that sample equal size instances from all classes and sampling the most representative instances from each class. In statistics, stratification is the process of dividing members of the population into homogeneous subgroups before sampling. We choose to use stratified sampling to sample instances from data's subpopulations because sampled instances cover all possible subpopulations and is a substantive reflection of the original data population.

However, it's non-trivial to find homogeneous subpopulations from a set of sequences x_t belonging to a particular class, because these sequences are often high-dimensional (in time steps) and noisy. Determining the number of clusters S is difficult for unknown data distribution. Fortunately, the parameter S is usually large for sampling tasks. For an example of our experiments, S is on a scale of 3K for a balanced training dataset that each class contains 10K instances. That is, around 30% of the instance population is sampled. We leverage the Hierarchical Agglomerative Clustering (HAC) that gradually calculates the increased distances between instances and newly formed dendrogram nodes in a bottom-up direction. The HAC iteration stops when the node size reaches S to save computation time. As illustrated in a native example in Figure 2d left, the iteration stops at the cut location (yellow line) where only nodes below the cut are computed. The algorithm then randomly sample an instance from each sub-cluster to form S samples in total. In Algorithm 1, the sampling procedure includes a computational efficient HAC algorithm in lines 3-20, except that line 10 is an iteration through $N - S$ instead of $N - 1$ as in the original HAC algorithm. If S is 30% of N for instance, the computation becomes $1 - 0.3 = 0.7$ time faster than looping through all N . Specifically, the algorithm uses extra memories to store the next-best-merge array NBM to improve the complexity [23]. The $Cluster()$ function in line 21 then converts the node linkage table A_1 to a tree structure and returns the clusters C_S , which stores the instance indices for each cluster. Line 24 implements the sampling algorithm explained above. We calculate a transformed L2-norm distance between instance a_i^T and a_j^T which have NULL entries as

$$dist(x_i^T, x_j^T) = \frac{\sqrt{\sum_{t=1}^T (x_i^t - x_j^t)^2}}{T}, \text{ if } x_i^t \neq \emptyset \text{ and } x_j^t \neq \emptyset \quad (3)$$

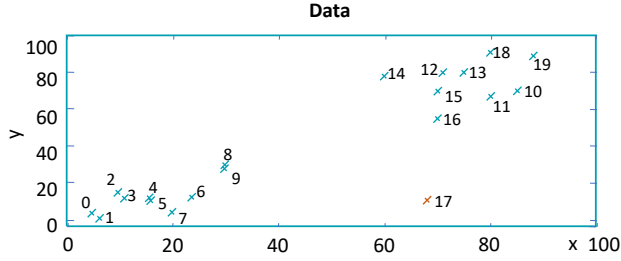
where the numerator is the shortest L2-norm distance between two hyper-planes formed by the non-null dimensions and the denominator penalizes non-null dimensions.

Using HAC-based stratified sampling benefits the attribution analysis from several properties. First, it guarantees enhanced precision and population depiction comparing to other sampling methods. Second, the sampling running time is inversely proportional to sample size K , and therefore faster than sampling with other clustering algorithms such as k-means when K is large. Comparing to k-means, HAC-based sampling methods do not have a convergence problem either. Third, the algorithm is scalable to the visual summary for a large dataset. Additionally, without data prerequisites such as particular distribution assumptions and high dimensional density, the method scales for different applications (**DG5**). Last but not least, stratified sampling is intimately coherent with the following within-class temporal pattern summarization.

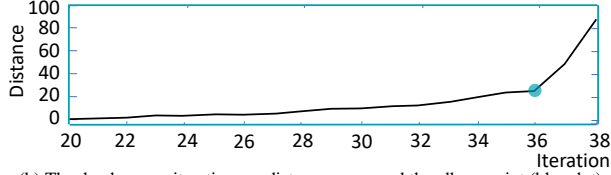
5.4 Within-Class Summary with NoRCE

In correspondence with **DG2**, ViSFA aims to provide sequence summaries for users to recognize temporally contributing patterns in each class. We introduce NoRCE – a systematical algorithm for noise reduction and the number of cluster estimation.

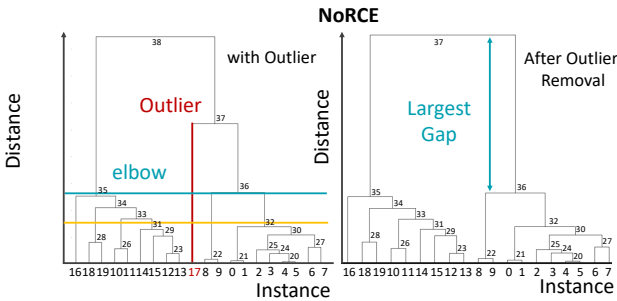
A few signature data properties brought challenges to summarizing sequence patterns. First, RNN training produces significant noise. Eliminating the influence of noise is essential before further operations. Besides, high-dimensional data is often sparse. Many algorithms are designed for dense datasets which will produce artifacts for sparse data analysis. We will show an example later.



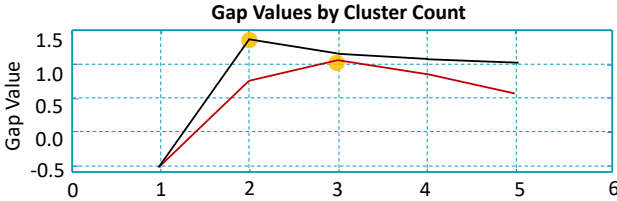
(a) Sample data that homogeneously form two clusters and an outlier (instance 17).



(b) The dendrogram iteration vs. distance curve and the elbow point (blue dot).



(c) A dendrogram illustration of HAC-based outlier removal. Left: original data, locating outlier 17 with dendrogram cutting. Right: new dendrogram forms after removing outlier. Numbers represent node IDs in sequential order.



(d) Optimal Cluster Size comparison before (red) and after (black) removing outlier.

Figure 2: Illustration of NoRCE in with a simple example.

Additionally, determining the number of clusters K is difficult for unknown data distribution. Although dimension reduction techniques such as t-SNE are often used to visualize data distribution, the visualized distribution is only an approximation. Visualizing dimension-reduced data can be misleading, especially when the feature dimension is high, due to the dimension curse. Determining the optimal K for such a dataset is more challenging. Because deep neural networks are still “blackbox,” it’s unclear whether sequences from each class would homogeneously form more than one group. NoRCE is designed to resolve these difficulties.

NoRCE first performs noise reduction. We present this procedure in lines 27-35 in Algorithm 1. Specifically, $HAC()$ is the HAC calculation function that returns the nodes’ linkage table A_2 created in the process. Figure 2 illustrates the concept of noise reduction using a simple 2D example, where the instances are shown in Figure 2a. Instance 17 ($I17$) is the outlier in the dataset that homogeneously forms two clusters on the bottom left and top right, respectively. During the HAC dendrogram building process, newly formed nodes have lower similarities to nearby nodes than early formed nodes, as shown in Figure 2c where node IDs are in progressive order where

nodes with smaller IDs form earlier and vice versa. Therefore, the dendrogram iteration vs. distance curve is monotone increasing. As shown in Figure 2b, the distance for the example dataset is monotone increasing during the iteration. As shown in Figure 2c left, the distance suddenly increases when $I17$ joins the bottom-up building process of the dendrogram. Meanwhile, the iteration-distance curve exhibits an elbow point where a sudden jump of distance value happens at iteration 36 that cut through $I17$ as shown by the horizontal blue line. This phenomenon is not a coincident in fact, as the outliers are distanced from other nodes. We then leverage this property and use the elbow point as a threshold to detect outliers which are the instances covered by dendrogram layers to the right of elbow point. In Algorithm 1, the $Distances()$ function on line 29 computes the iteration-distance curve from A_2 . And NoRCE computes the elbow point by smoothing the curve and find the maximum absolute second derivative, as shown on line 30. As illustrated in Figure 2c left, the algorithm detects $I17$ as an outlier because it’s the single instance whose closest distance to other instances is greater than the elbow point. NoRCE computes the elbow point by smoothing the curve and find the maximum absolute second derivative, as shown on line 30. Users can also adjust the elbow point interactively, which is introduced in section 5.6.

After removing the outliers, NoRCE introduces an Adaptive Gap Statistic (AGS) algorithm to estimate the number of clusters. Gap Statistic (GS) [42] is a method for determining the number of clusters in a set of data by comparing the within-cluster dispersion to its expectation under an appropriate reference distribution of data. The GS method is proved to outperforms other numbers of cluster estimating methods, such as the average silhouettes method [34] and the elbow methods [16]. Figure 2d shows the results of the gap statistic before (red) and after (black) removing the outlier. The estimated cluster numbers are correspondence with the most significant gap values (yellow). After removing the outlier, the algorithm automatically detects two optimal clusters with the cut that splits the largest gap in the dendrogram, as shown in Figure 2d right.

We show the AGS algorithm in lines 36-56 in Algorithm 1. AGS takes two parameters: the number of references N_{ref} and the maximum cluster number K_{max} , and returns the estimated number of cluster $OptK$. We set $N_{ref} = 3$ and $K_{max} = 15$ in our experiments. The classic gap statistic algorithm creates randomized data reference that is within the original data range. However, for high-dimensional sparse data, such references often greatly change the original data distribution and lead to unreasonable cluster number estimation. Imagine a dataset where all instances are individual points in a 3D space. Sparse data indicates that most points in this space are on the planes made by two axes or on one of the axes. However, randomly generated data would evenly distribute in the 3D space, which is different from the sparse data distribution. Then the question is how to reference data that has similar distribution? Fortunately, NoRCE’s input Y is sampled from the original training data X . As shown in line 44 in Algorithm 1, function $AdaptiveReferencing()$ randomly samples the same number of instances as Y from the residual data $X - Y$ as references. Then computes the gap values through the for loops and returns the optimal cluster number $OptK$, which correspondences with the largest gap value. Finally, line 56 computes the estimated clusters for later visualization. Specifically, users can also adjust the number of clusters interactively. We introduced more details in the next section.

5.5 Visualization Design

In this subsection, we focus on the visualization of contributing temporal pattern summaries and their comparison between prediction classes, based on the algorithm presented in the previous subsection.

Algorithm 1 Contributing Sequence Pattern Summary for RNN Predictions

```

1: procedure STRATIFIEDSAMPLING( $\langle x_1, \dots, x_N \rangle, S$ )
2:    $Y$ , number of samples
3:   for  $j \leftarrow 1 : N$  do
4:     for  $i \leftarrow 1 : N$  do
5:        $C[j][i].sim \leftarrow \text{Similarity}(x_i, x_j)$ 
6:        $C[j][i].index \leftarrow i$ 
7:        $I[j] \leftarrow j$  ▷  $I$  tracks active clusters
8:        $NBM[j] \leftarrow \text{argmax}_{X \in C[j][i]; j \neq i} X.sim$ 
9:      $A_1 \leftarrow []$ 
10:    for  $n \leftarrow 1 : N - S$  do
11:       $i_1 \leftarrow \text{argmax}_{i: I[i]=j} NBM[i].sim$ 
12:       $i_2 \leftarrow I[NBM[i_1].index]$ 
13:       $A_1.Append(\langle i_1, i_2 \rangle)$ 
14:      for  $i \leftarrow 1 : N$  do
15:        if  $I[i] = i \wedge i \neq i_1 \wedge i \neq i_2$  then
16:           $C[i][i_1].sim \leftarrow \max(C[i][i_1][i].sim, C[i_2][i].sim)$ 
17:           $C[i][i_2].sim \leftarrow C[i][i_1].sim$ 
18:        if  $I[i] = i_2$  then
19:           $I[i] \leftarrow i_1$ 
20:           $NBM[i_1] \leftarrow \text{argmax}_{X \in C[i_1][i]; I[i]=i \wedge i \neq i_1} X.sim$ 
21:       $C_S \leftarrow \text{Clusters}(A_1)$ 
22:       $W \leftarrow []$ 
23:      for  $s \leftarrow i, S$  do
24:         $W.Append(\text{RandomSample}(C_S[s]))$ 
25:      return  $W$ 
26: procedure NoRCE( $W, \langle x_1, \dots, x_N \rangle$ )
27:   procedure NOISEREDUCTION( $W$ )
28:      $A_2 \leftarrow HAC(W)$  ▷ Run HAC on  $W$ , return  $A_2$ 
29:      $d \leftarrow \text{Distances}(A_2)$  ▷ Converts table  $A_2$  to tree
30:      $ELBOW \leftarrow \text{argmax}_{index} \text{SecondDerivative}(\text{Smooth}(d(index)))$ 
31:      $Y \leftarrow []$  ▷ leaf nodes before elbow
32:     for  $i \leftarrow A_2[1 : ELBOW]$  do
33:       if  $i \neq S - 1$  then
34:          $Y.Append(i)$ 
35:     return  $Y$ 
36:   procedure ADAPTIVE GAP STATISTICS( $\langle x_1, \dots, x_N \rangle, Y$ )
37:      $N_{ref}$ , number of references
38:      $K_{max}$ , maximum number of clusters
39:      $A_3 \leftarrow HAC(Y)$ 
40:      $Gaps \leftarrow []$ 
41:     for  $index, K \leftarrow 1 : K_{max}$  do
42:        $W'_{ks} \leftarrow []$ 
43:       for  $i = 1 : N_{ref}$  do
44:          $Y' \leftarrow \text{AdaptiveReferencing}(X, Y.size)$ 
45:          $A' \leftarrow HAC(Y')$ 
46:          $clusterLabels' \leftarrow \text{CutTree}(A', k)$ 
47:          $\mu'_k, C'_k \leftarrow \text{ComputeCenters}(Y', clusterLabels')$ 
48:          $W'_{ks}[i] \leftarrow \log \sum_{k=1}^K \sum_{x_i \in C'_k} \|x_i - \mu'_k\|^2$ 
49:        $W'_k \leftarrow \sum_{i=1}^{N_{ref}} W'_{ks}$ 
50:        $clusterLabels \leftarrow \text{CutTree}(A_3, k)$ 
51:        $\mu_k, C_k \leftarrow \text{ComputeCenters}(Y, clusterLabels)$ 
52:        $W_k \leftarrow \sum_{k=1}^K \sum_{x_i \in C_k} \|x_i - \mu_k\|^2$ 
53:        $Gap_k \leftarrow W'_k - \log W_k$ 
54:        $Gaps.Append(Gap_k)$ 
55:        $OptK \leftarrow \text{argmax}_k Gaps[k]$ 
56:     return  $OptK$ 
57:    $OptClusters \leftarrow \text{CutTree}(A_3, OptK)$ 

```

5.5.1 Dashboard

We visualize the statistical distributions of instance properties in a dashboard, as shown on the left of Figure 3. To provide users with an overview, the projection view embeds the high-dimensional temporal feature sequences into a two-dimensional canvas via t-SNE [22] (see Figure 3a). The dimension reduction result can reflect the similarity of instances in a rough way. Besides, instance attribute information is indispensable for users to draw conclusions. For example, doctors always need to know patients’ gender and age before diagnosis. ViSFA lists bar charts in the attribute view (see Figure 3b for all instance attributes (not including temporal features). Specially, we employ a contrast color pair to encode the bars for two classes. This color scheme is applied in the entire ViSFA system.

5.5.2 Temporal Pattern View

ViSFA illustrates the over-time feature value change in the temporal pattern view, as shown in Figure 3c. AttentionHeatmap [43] overlays contributing temporal events in a time-value plane. Such design has perception issues, such as line crossing hinders users to notice jump over edges. In this work, the temporal pattern view visualizes the NoRCE clustering results using stacked area charts.

Dendrograms, as shown in Figure 2b, illustrate the clustering loss of each iteration by distance on the vertical axis. However, it is unnecessary for users to distinguish each individual by ID on the horizontal axis. Thus, we employ a line chart with an iteration axis (horizontal) and a distance axis (vertical), as shown in Figure 3c1. Two curves for different classes are placed together for comparison. Actually, the curves in such a line chart can give hints to set the elbow point to users—a dramatic increase of distance between the instances is a good choice for noise reduction. We also illustrate the curve segments right to the elbow point by dashed lines, which implies that the instances clustered in the later iterations will be regarded as noise.

We visualize the denoised instances from two classes in a juxtaposition layout for easy comparison [11]. To highlight the dominant patterns in the instances, we sort the clusters belonging to each class in size descending order from top to bottom. Besides, the clusters, whose sizes are far less than the biggest cluster, are collected into a group called “small clusters.” For each class, we design a size summary chart as shown in Figure 3c2, and a series of temporal pattern summary charts as shown in Figure 3c3. In the size summary chart, we provide two scale functions to adapt to different comparison needs: log scales to show all clusters together, and linear scales to compare the clusters in the small clusters.

ViSFA lists a temporal pattern summary chart for each cluster, except for the small ones. To save space, the description of the small clusters are merged into the same chart. But they can be checked alone by hovering the related bar in the size summary chart. In each temporal pattern summary chart, the cluster is summarized as a median line and a stream flowing over time (horizontal axis). The trend and the width of the stream are defined by feature value ranges mapped to the vertical axis.

To avoid over-extending ranges caused by outliers, we color the stream with different opacity based on its quantiles. If a wide stream has a narrow dark stream, users will know that there must be one or more outliers. Besides, wide streams may mislead users to believe that there exist many individual values. We encode the number of instances at each time-step with a bar chart on the top of each temporal pattern summary chart. For some time points or time segments, our model considers no values as important (the bottom row in Figure 3c3), thus the stream may have breaks. The bars can facilitate users in detecting breaks and narrow streams. However, the time points isolated by two breaks may still be ignored by users. To highlight the streams for such time points, we extend the streams toward their neighboring points.

To demonstrate temporal patterns involving two features, AttentionHeatmap [43] applies two-hierarchy axis, which is not intuitive to read values or compare trends over time. ViSFA improves the design by placing the axes for the two features symmetrically, as shown in Figure 4. It is convenient to discover relationships from a symmetrical design.

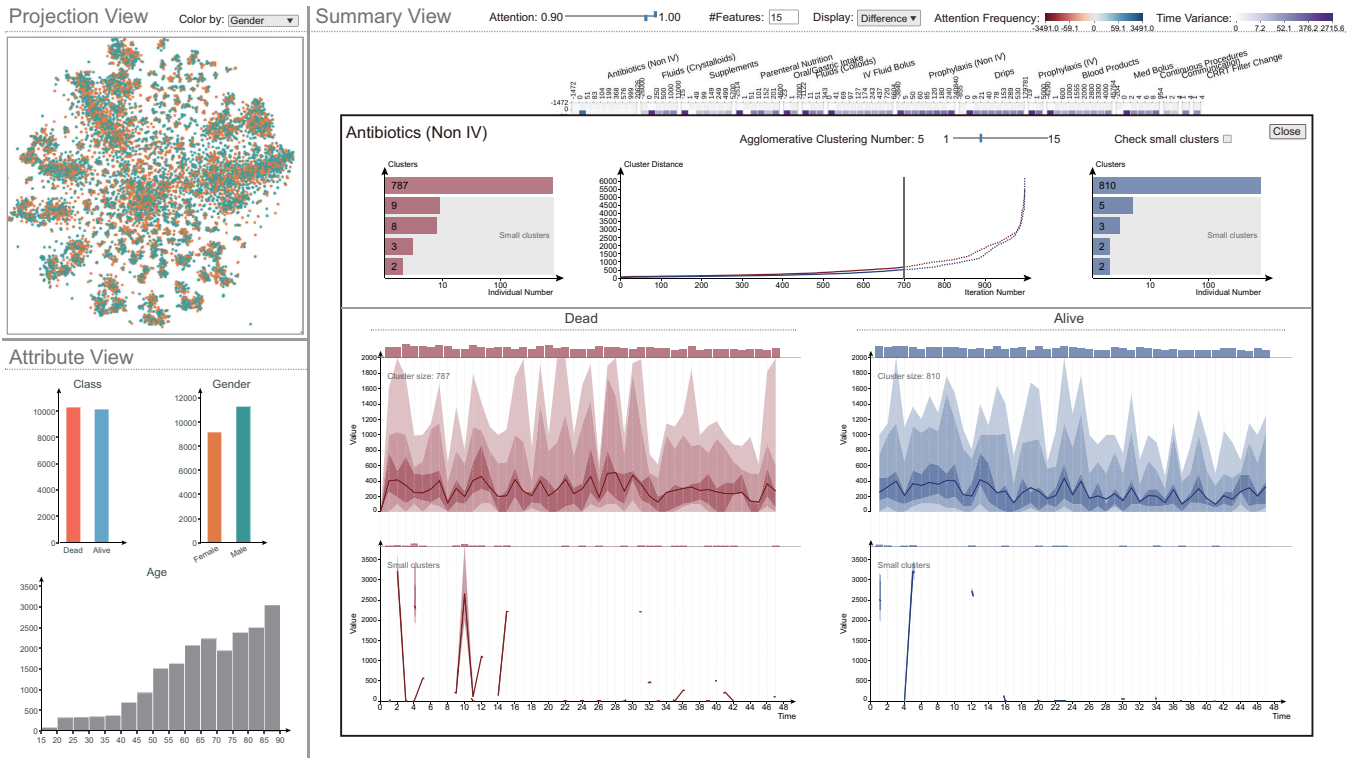


Figure 3: The interface of ViSFA is composed of 1) a dashboard including a projection view (a) and an attribute view (b), and 2) a summary view, which is initialized as a matrix grid view. Clicking a cell in the matrix grid can trigger the corresponding temporal pattern view (c).

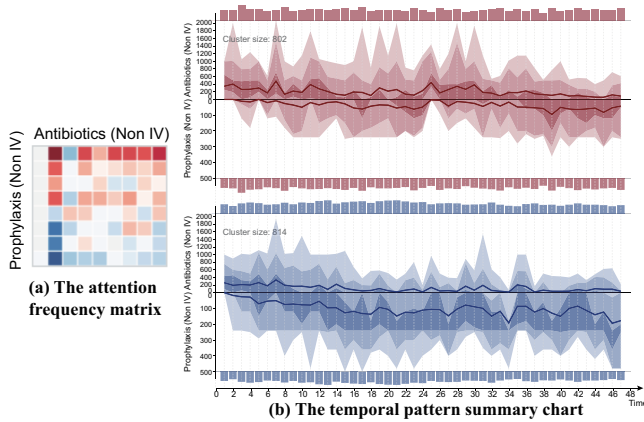


Figure 4: The matrix grid cell (a) of “Antibiotics (Non IV)” and “Prophylaxis (Non IV)” and the related temporal pattern summary chart (b), comparing the feature value trends of the two features between the biggest clusters in two classes.

5.6 Interaction Methods

ViSFA provides multiple interactions for user to explore data and discover insights.

Filter by attention. The two-level neural attention model calculates the attention of events based on their importance. Taking this advantage, ViSFA has a chance to filter the results shown in the matrix grid view and the temporal pattern view according to the model-generated attention. The filter range can be set by users via a slide bar.

Check temporal patterns. The temporal pattern view can be triggered by clicking a cell in the matrix grid view. The cells on the diagonal correspond to temporal patterns with a single feature, and

the other cells correspond to temporal patterns with two features. In the temporal pattern view, users can drag a vertical line to adjust the iteration stop and the number of clusters.

Remove noise. It is challenging to decide which records are noise for various datasets by automatic models. Different decisions may lead to distinct results in the latter analysis [31]. Thus, we allow users to set the parameter for noise removing by dragging a dashed line in the line chart illustrating HAC, as shown in Figure 3a.

Set cluster number. The initialized cluster number is the result of AGS. However, the model-defined cluster number may be unsatisfying for distinct application scenarios [17]. Users can adjust the cluster number via a slider.

Check characteristics of instances belonging to a single cluster. The instances in the same cluster may have similar characteristics. For instance, there may exist special treatments for elderly patients. To help users figure out if there exists such a phenomenon, the dashboard highlights the instances belonging to the cluster selected from the temporal pattern view.

6 EXPERIMENTS AND RESULTS

We verified the effectiveness of our approach with two open datasets. The first dataset is from the medical domain for studying patients mortality study. The second dataset is from the education domain for studying students’ learning activities. We showcase the visual analytics results and discover insights in the following subsections.

6.1 EHR Data

The development of ViSFA is motivated by the needs of ICU patients’ mortality analysis. We first validate ViSFA with the MIMIC [13] dataset. We train an RNN model using four categories of patients’ information – ICU stay, inputs, procedure and lab results. This information contains 37 temporal features, as shown in table 1. The successfully trained model is able to use patients’ records in the first 48 hours after admission to predict their mortalities after 48

Table 1: MIMIC Features Used in Mortality Prediction

Category	Features
ICU	ICU Stay Length
Input	Drips, Antibiotics (Non IV), Fluids (Crystalloids), Supplements, Pre Admission, Med Bolus, Insulin (Non IV), Parenteral Nutrition, Oral/Gastric Intake, Fluids (Colloids), Prophylaxis (IV), Antibiotics (IV), IV Fluid Bolus, Prophylaxis (Non IV), Enteral Nutrition, Blood Products
Procedure	Peritoneal Dialysis, Continuous Procedures, Dialysis, Intubation/Extubation, Communication, CRRT Filter Change, Invasive Lines, Ventilation, Significant Events, Peripheral Lines, Procedures, Imaging
Labs	Other Body Fluid, Joint Fluid, Pleural, Cerebrospinal Fluid (CSF), Urine, Ascites, Stool, Blood

hours. The analysis task is to find what features and values among all features contribute most to mortality predictions and what is the difference of temporal patterns in contributing feature values between mortality prediction classes. The preprocessed dataset contains 14K patients, a.k.a instances, where the alive/dead patient ratio is 10:1. We train the model using the oversampling technique and therefore the data for final analysis contain 24K instances. 10% data are sampled in the stratified sampling procedure.

The matrix grid (Figure 1 in the supplementary material) shows the top six contributing features. Most top-ranked features are inputs, which indicate inputs are more important in keep patients alive comparing to ICU events, procedures, and lab tests. This is reasonable as fluids affect the cardiovascular, renal, gastrointestinal, and immune systems in critical illness treatment [24]. We reveal more case study results regarding the matrix grid view in the supplementary material.

Figure 3c shows the summary of temporal changes in feature “Antibiotics (Non IV)”. The largest clusters contain more than 800 instances after removing temporal events of low attentions and noise reduction. All percentiles (15, 25, 40, 60, 75, 85) and the average lines have uniform temporal fluctuations for both classes. This phenomenon demonstrates the effectiveness of the NoRCE algorithm. The concentrated major cluster further validates that ViSFA distills major contributing patterns among large datasets. We can notice several phenomenons from the visual comparison results. First, the contributing temporal events for patients in the dead class show higher antibiotic levels throughout the entire time period comparing to the alive class. According to the domain scientist, combining antibiotics is a strategy often used by clinicians, but recent research shows that such a strategy can cause body resistance [6]. Also, there is research demonstrating that deploying synergistic antibiotics can, in practice, be the worst strategy if bacterial clearance is not achieved after the first treatment phase [29], which can be the explanation of the phenomenon. Second, the antibiotic dosage for two classes both fluctuated throughout time, but their temporal patterns show significant differences. For instance, the alive class feature in a relatively more steady fluctuation compared to the dead class, which shows more significant peaks and bumps. Specifically, the first great drop of value happens at 4h for the alive class but happens at 8h for the dead class. Both classes have fluctuated patterns around 24h ($\pm 2h$). However, the alive class shows a more steady change afterward while the dead class shows two significant peaks in the next six hours, and the dosage becomes steady afterward. The domain scientist who participated in the case study indicates that she is highly interested in the visualized result, and the comparative temporal pattern visualization is very informative. Although she can not verify the cause of antibiotics dosage change on every time point without further experiments, she states the visual summaries could potentially reveal critical time points in the patient treatment process. Besides, she mentioned that the suddenly increased values in the last two hours for the dead group are highly reasonable because the

previous antibiotics were not effective enough.

6.2 Open University Learning Analytics Dataset

Here, we demonstrate ViSFA is applicable to different applications with the open university learning analytics (OULAD) dataset [18]. OULAD collects the clickstream data of students’ interactions in the virtual learning environment (VLE). The purpose is to study students’ contributing learning behavior to different course evaluation results – pass and fail. The training data is balanced that the numbers of students from both classes are approximately equal. We train an RNN model using the number of clicks on 20 VLE page categories for 1678 students in 285 days. The trained binary prediction model is able to forecast a student’s course evaluation result. The webpage categories includes homepage, course contents, collaboration assignments, quiz, glossary, forum, supplementary contents, etc.

The feature contribution ranking results (Figure 1 in the supplementary material) indicate that “forum,” “contents” (both course and supplementary) and “quizzes” have the most significant contributions among all page types. Contrarily, pages such as “glossary” and “additional data” are the least contributing pages. The matrix-grid view generated with the new model indicates that forum participation is also one of the top important features in achieving desired course evaluations. Evidently, high participation in the forum is effective in achieving satisfying course evaluations. Studies show that peer learning can enhance learning outcomes such as increased motivation and engagement in the learning task, deeper levels of understanding, increased metacognition, the development of higher-order thinking skills and divergent thinking [4, 41]. And the pages like “glossary” and “additional data” are obviously less related to a course evaluation and thus rank lower.

We then invest in students’ overtime learning behaviors. Figures 5a and 5b show the change in contributing features “course content” and “forum,” respectively. The comparison between the “passed” and “failed” classes reveals that students who achieve satisfying course evaluation spend about three times in the course contents and forum discussions than students who fail in the course. Previous study [7] shows that students who failed in their courses tended to interact less frequently. The results in Figure 5 not only supports the argument but also provides evidence that “failed” students interacted less both on a daily basis and in the long term.

Interestingly, students tend to have different over-time interaction patterns between course contents and forum participation. The quantile lines show normal distribution like patterns for course contents, while the curves for the forum are like chi-square distributions. These phenomenons indicate that students tend to participate more in forum discussions at the beginning of the learning period, and the participation becomes lower after about ten days. As one might expect, students usually have more questions at the beginning. Meanwhile, “passed” students access to course contents in a gradually increasing and then progressively decreasing manner. However, the interaction for “failed” students tends to decrease quickly from the very beginning with a much lower participation amount comparing to the “passed” class. These phenomenons again illustrate the importance of devotion and participation during online learning in achieving desired course grades.

The temporal pattern summary charts in Figure 5 show that most meaningful events happen in the first 180 days (one semester). The bar charts on the top of Figure 5a left and Figure 5a left also reveal that the learned prediction model distinguishes the “fail” class by only judging if the numbers of clicks are zeros after 60 days. Therefore, we retrain an RNN model using the first 180 days of the data. The temporal summary charts compute from the new model are shown in Figure 6. Naturally, the visualization from the new model shows more details that better contrast two classes because the new model is learned with training data that discard the noisy and less informative time-steps.

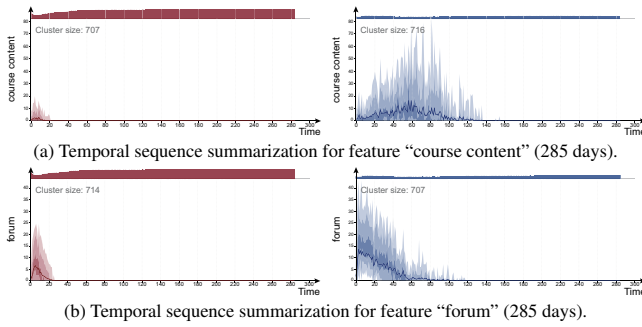


Figure 5: Temporal patterns in contributing features (285 days).

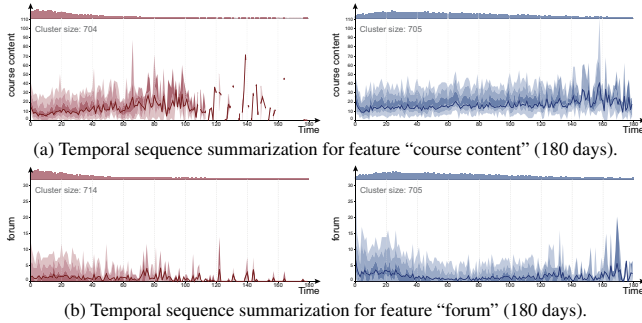


Figure 6: Temporal patterns in contributing features (180 days).

In Figure 6a and Figure 6b, the percentile and average sequences have a more uniform tendency comparing to Figure 5. The results in Figure 6 also indicates that the learning pattern in the first half of a semester is more important than the second half, as shown in all bar charts on the top. Meanwhile, students who passed the course tend to have twice access to both the content and the forum, and these patterns are considered highly contributing to the prediction. The results further emphasize the importance of engagement of course contents and forum discussions. The experiments demonstrate the temporal summary view can help verify RNN model reliability and provide guidance for retraining a better model.

The matrix-grid view generated with the new model (Figure 2 in the supplementary materials) also indicates the importance of the pages directly related to course materials such as “contents,” “resources,” and “course supplementary contents.” We showcase more case study results in the supplementary materials.

7 DISCUSSION

During the exploration of feature attribution for two fundamentally distinctive datasets, we found a mutual phenomenon that there is always a **dominant concentrate cluster**. Enlarging cluster number hardly changes the domination, and only small clusters appear in the bottom, as shown in Figure 3. The NoRCE computation results also verify this phenomenon that the estimated cluster number is one in most experiments. We consider the mutual temporal patterns in the dominant cluster as the important facts that contribute to distinguishing two prediction classes. These facts can be complex, as illustrated in the EHR data analysis where domain expert suggests more longitudinal experiments are required to verify its reliability. And the facts can be straightforward to understand and explain, as shown in the OULAD data analysis. However, we can not conclude that RNN models always learn one dominant pattern for each feature without abundant experiments in various application domains. Therefore, we design the temporal view so that the analysis is feasible for visualizing more large clusters.

Causality vs correlation. Although our approach can visualize features and their overtime patterns contributing to class predictions,

it’s inadequate to consider top-ranked features and their overtime patterns the cause to the predicted class. The learned attribution reflects what features/values in the training dataset significantly correlated to the prediction whereas causation indicates that the labeled class is the result of the features, which is a stronger statement to prove and beyond the scope of our discussion.

However, although it’s insufficient for causal analysis, feature attribution analysis provides evidence for further causal analysis. For example, students’ behavior learned by RNN can not be proved to cause their course evaluation results without further controlled experiments [28]. But our approach uncovers important pages and students’ interactive temporal patterns that are correlated with the course evaluation results. Similarly, the antibiotics (Non-IV) doses applied to the patients who died after 48 hours are not necessarily the cause of their death. But the analysis provides statistically supportive evidence that different doses of antibiotics (Non-IV) are correlated with patients mortality.

The ViSFA system uses a **modular design** where the stratified sampling module is for scalable and comparative analysis, and the NoRCE module is for noise reduction and temporal pattern summarization. ViSFA also provides a systematic framework containing these modules to motivate more discussions to probe RNN classifiers behavior in the value-level. As discussed in the related work section, the proposed analysis can be used to a broad range of sequence analysis scenarios and the noise removal and the pattern summarization modules are two requisite steps in the analysis.

8 CONCLUSION

As deep learning pervasively used in decision-making tasks for multidimensional sequential data analysis, it’s essential to understand contributing features and temporal patterns for predictions. In this work, we present ViSFA, the first visual analytics system that scalably summarizes value-level feature attributions with recurrent neural attention networks. We test ViSFA with two real-world datasets. The case study results demonstrate that ViSFA can help effectively reason value-level feature attribution for different application domains, and the visual summaries of temporal patterns in feature attribution provide guidelines for making future decisions. We hope our work will motivate further research in developing domain-user-oriented analysis systems with deep learning.

9 CONCLUSION

As deep learning pervasively used in decision-making tasks for multidimensional sequential data analysis, it’s essential to understand contributing features and temporal patterns for predictions. In this work, we present ViSFA, the first visual analytics system that scalably summarizes value-level feature attributions with recurrent neural attention networks. We test ViSFA with two real-world datasets. The case study results demonstrate that ViSFA can help effectively reason value-level feature attribution for different application domains, and the visual summaries of temporal patterns in feature attribution provide guidelines for making future decisions. We hope our work will motivate further research in developing domain-user-oriented analysis systems with deep learning.

ACKNOWLEDGMENTS

The authors wish to thank A, B, and C. This work was supported in part by a grant from XYZ.

REFERENCES

- [1] D. Bahdanau, K. Cho, and Y. Bengio. Neural machine translation by jointly learning to align and translate. In *Proceedings of the 3rd International Conference on Learning Representations*, 2015.
- [2] W. Bao, J. Yue, and Y. Rao. A deep learning framework for financial time series using stacked autoencoders and long-short term memory. *PLoS ONE*, 12(7):e0180944, 2017.

- [3] A. Bilal, A. Jourabloo, M. Ye, X. Liu, and L. Ren. Do convolutional neural networks learn class hierarchy? *IEEE Transactions on Visualization and Computer Graphics*, 24(1):152–162, 2018.
- [4] P. C. Blumenfeld, R. W. Marx, E. Soloway, and J. Krajcik. Learning with peers: From small group cooperation to collaborative communities. *Educational Researcher*, 25(8):37–39, 1996.
- [5] E. Choi, M. T. Bahadori, J. Sun, J. Kulas, A. Schuetz, and W. Stewart. Retain: An interpretable predictive model for healthcare using reverse time attention mechanism. In *Proceedings of Annual Conference on Neural Information Processing Systems*, pp. 3504–3512. Curran Associates, Inc., 2016.
- [6] G. D. Wright. Antibiotic adjuvants: Rescuing antibiotics from resistance. *Trends in Microbiology*, 24(11):862–871, 2016.
- [7] J. Davies and M. Graff. Performance in e-learning: Online participation and student grades. *British Journal of Educational Technology*, 36:657–663, 2005.
- [8] Y. Ding, Y. Liu, H. Luan, and M. Sun. Visualizing and understanding neural machine translation. In *Proceedings of the 55th Annual Meeting of the Association for Computational Linguistics*, pp. 1150–1159, 2017.
- [9] F. Doshi-Velez and B. Kim. Towards a rigorous science of interpretable machine learning. In *eprint arXiv:1702.08608*, 2017.
- [10] P. E. Rauber, S. Fadel, A. X. Falco, and A. Telea. Visualizing the hidden activity of artificial neural networks. *IEEE Transactions on Visualization and Computer Graphics*, 23(1):101–110, 2016.
- [11] M. Gleicher, D. Albers, R. Walker, I. Jusufi, C. D. Hansen, and J. C. Roberts. Visual comparison for information visualization. *Information Visualization*, 10(4):289–309, 2011.
- [12] K. M. Hermann, T. Kociský, E. Grefenstette, L. Espeholt, W. Kay, M. Suleyman, and P. Blunsom. Teaching machines to read and comprehend. In *Advances in Neural Information Processing Systems*, 2015.
- [13] A. E. Johnson, T. J. Pollard, L. Shen, H. L. Li-wei, M. Feng, M. Ghassemi, B. Moody, P. Szolovits, L. A. Celi, and R. G. Mark. Mimic-iii, a freely accessible critical care database. *Scientific data*, 3:160035, 2016.
- [14] M. Kahng, P. Y. Andrews, A. Kalro, and D. H. Chau. Activis: Visual exploration of industry-scale deep neural network models. *IEEE Transactions on Visualization and Computer Graphics*, 24(1):88–97, 2017.
- [15] A. Karpathy, J. Johnson, and F. Li. Visualizing and understanding recurrent networks. *CoRR*, abs/1506.02078, 2015.
- [16] D. J. KETCHEN and C. L. SHOOK. The application of cluster analysis in strategic management research: An analysis and critique. *Strategic Management Journal*, 17(6):441–458, 1996.
- [17] Y.-I. Kim, D.-W. Kim, D. Lee, and K. H. Lee. A cluster validation index for gk cluster analysis based on relative degree of sharing. *Information Sciences*, 168(1-4):225–242, 2004.
- [18] J. Kuzilek, M. Hlosta, and Z. Zdrahal. Open university learning analytics dataset. *Scientific Data*, 4(170171), 2017.
- [19] B. C. Kwon, M. Choi, J. T. Kim, E. Choi, Y. B. Kim, S. Kwon, J. Sun, and J. Choo. Retainvis: Visual analytics with interpretable and interactive recurrent neural networks on electronic medical records. *IEEE Transactions on Visualization and Computer Graphics*, 25(1), 2019.
- [20] J. Li, X. Chen, E. Hovy, and D. Jurafsky. Visualizing and understanding neural models in NLP. In *Proceedings of the 2016 Conference of the NAACL: Human Language Technologies*, pp. 681–691. Association for Computational Linguistics, San Diego, California, 2016.
- [21] S. M. Lundberg and S.-I. Lee. A unified approach to interpreting model predictions. In I. Guyon, U. V. Luxburg, S. Bengio, H. Wallach, R. Fergus, S. Vishwanathan, and R. Garnett, eds., *Proceedings of Annual Conference on Neural Information Processing Systems*, pp. 4765–4774, 2017.
- [22] L. v. d. Maaten and G. Hinton. Visualizing data using t-sne. *Journal of machine learning research*, 9(Nov):2579–2605, 2008.
- [23] C. D. Manning, P. Raghavan, and H. Schütze. *Introduction to Information Retrieval*. Cambridge University Press, 2008.
- [24] C. Martin, A. Cortegiani, C. Gregoretti, I. Martin-Loeches, C. Ichai, M. Leone, G. Marx, and S. Einaiv. Choice of fluids in critically ill patients. *BMC Anesthesiology*, 18(1):200, 2018.
- [25] Y. Ming, S. Cao, R. Zhang, Y. Li, Y. Chen, Y. Song, and H. Qu. Understanding hidden memories of recurrent neural networks. In *Proceedings of 2017 IEEE Conference on Visual Analytics Science and Technology*, pp. 13–24, 2017.
- [26] Y. Ming, P. Xu, H. Qu, and L. Ren. Interpretable and steerable sequence learning via prototypes. In *Proceedings of the 25th ACM SIGKDD International Conf. on Knowledge Discovery and Data Mining*, 2019.
- [27] C. Olah, A. Mordvintsev, and L. Schubert. Feature visualization. *Distill*, 2(11):e7, 2017.
- [28] J. Pearl. *Causality: Models, Reasoning and Inference*. Cambridge University Press, 2nd ed., 2009.
- [29] R. Pena-Miller, D. Laehnemann, G. Jansen, A. Fuentes-Hernandez, P. Rosenstiel, H. Schulenburg, and R. Beardmore. When the most potent combination of antibiotics selects for the greatest bacterial load: The smile-frown transition. *PLoS Biology*, 11(4):e1001540, 2013.
- [30] D. Quang and X. Xie. Danq: A hybrid convolutional and recurrent deep neural network for quantifying the function of dna sequences. *Nucleic Acids Research*, 44:226, 2016.
- [31] J. R. Quinlan. Induction of decision trees. *Machine learning*, 1(1):81–106, 1986.
- [32] P. E. Rauber, S. G. Fadel, A. X. Falco, and A. C. Telea. Visualizing the hidden activity of artificial neural networks. *IEEE Transactions on Visualization and Computer Graphics*, 23(1):101–110, 2017.
- [33] M. T. Ribeiro, S. Singh, and C. Guestrin. Why should i trust you?: Explaining the predictions of any classifier. In *Proceedings of the 22nd ACM SIGKDD International Conference on Knowledge Discovery and Data Mining*, pp. 1135–1144, 2016.
- [34] P. Rousseeuw. Silhouettes: A graphical aid to the interpretation and validation of cluster analysis. *Journal of Computational and Applied Mathematics*, 20(1):53–65, 1987.
- [35] C. Rudin. Stop explaining black box machine learning models for high stakes decisions and use interpretable models instead. *Nature Machine Intelligence*, 1(5):206–215, 2019.
- [36] H. Sheil, O. Rana, and R. G. Reilly. Predicting purchasing intent: Automatic feature learning using recurrent neural networks. In *Proceedings of the SIGIR 2018 Workshop on eCommerce co-located with the 41st International ACM SIGIR Conference on Research and Development in Information Retrieval*, 2018.
- [37] A. Shrikumar, P. Greenside, and A. Kundaje. Learning important features through propagating activation differences. In *Proceedings of the 34th International Conference on Machine Learning*, vol. 70, pp. 3145–3153. Proceedings of Machine Learning Research, 2017.
- [38] A. Shrikumar, P. Greenside, A. Shcherbina, and A. Kundaje. Not just a black box: Learning important features through propagating activation differences. *arXiv*, 2016.
- [39] K. Simonyan, A. Vedaldi, and A. Zisserman. Deep inside convolutional networks: Visualising image classification models and saliency maps. *CoRR*, abs/1312.6034, 2013.
- [40] H. Strobelt, S. Gehrmann, H. Pfister, and A. M. Rush. Lstmvis: A tool for visual analysis of hidden state dynamics in recurrent neural networks. *IEEE TVCG*, 24:667–676, 2016.
- [41] M. Thomas. Learning within incoherent structures: The space of online discussion forums. *Journal of Computer Assisted Learning*, 18:351–366, 2002.
- [42] R. Tibshirani, G. Walther, and T. Hastie. Estimating the number of clusters in a dataset via the gap statistic. *Journal of the Royal Statistical Society*, 63:411–423, 2000.
- [43] C. Wang, T. Onishi, K. Nemoto, and K. Ma. Visual reasoning of feature attribution with deep recurrent neural networks. In *IEEE International Conference on Big Data, Big Data 2018*, pp. 1661–1668, 2018.
- [44] K. Xu, J. L. Ba, R. Kiros, K. Cho, A. Courville, R. Salakhutdinov, R. S. Zemel, and Y. Bengio. Show, attend and tell: Neural image caption generation with visual attention. In *Proceedings of the 32nd International Conference on Machine Learning*, vol. 37, pp. 2048–2057. JMLR, 2015.
- [45] T. Young, D. Hazarika, S. Poria, and E. Cambria. Recent trends in deep learning based natural language processing. *IEEE Computational Intelligence Magazine*, 13(3):55–75, 2018.
- [46] J. Zhang, Y. Wang, P. Molino, L. Li, and D. S. Ebert. Manifold: A model-agnostic framework for interpretation and diagnosis of machine learning models. *IEEE Transactions on Visualization and Computer Graphics*, 25(1):364–373, 2019.